

Thickness-dependent magnetic properties and strain-induced orbital magnetic moment in SrRuO₃ thin films

K. Ishigami,¹ K. Yoshimatsu,² D. Toyota,² M. Takizawa,¹ T. Yoshida,¹ G. Shibata,¹ T. Harano,¹ Y. Takahashi,¹ T. Kadono,¹ V. K. Verma,¹ V. R. Singh,¹ Y. Takeda,³ T. Okane,³ Y. Saitoh,³ H. Yamagami,³ T. Koide,⁴ M. Oshima,² H. Kumigashira,^{2,4} and A. Fujimori^{1,5,3}

¹*Department of Physics, University of Tokyo, Bunkyo-ku, Tokyo 113-0033, Japan*

²*Department of Applied Chemistry, The University of Tokyo, Bunkyo-ku, Tokyo 113-8656, Japan*

³*Quantum Beam Science Directorate, Japan Atomic Energy Agency, Sayo, Hyogo 679-5148, Japan*

⁴*Photon Factory, IMSS, High Energy Accelerator Research Organization, Tsukuba, Ibaraki 305-0801, Japan*

⁵*Department of Complexity Science and Engineering, The University of Tokyo, Kashiwa, Chiba 277-0882, Japan*

(Dated: November 6, 2018)

Thin films of the ferromagnetic metal SrRuO₃ (SRO) show a varying easy magnetization axis depending on the epitaxial strain and undergo a metal-to-insulator transition with decreasing film thickness. We have investigated the magnetic properties of SRO thin films with varying thicknesses fabricated on SrTiO₃(001) substrates by soft x-ray magnetic circular dichroism (XMCD) at the Ru M_{2,3} edge. Results have shown that, with decreasing film thickness, the film changes from ferromagnetic to non-magnetic around 3 monolayer thickness, consistent with previous magnetization and magneto-optical Kerr effect measurements. The orbital magnetic moment perpendicular to the film was found to be $\sim 0.1 \mu_B/\text{Ru}$ atom, and remained nearly unchanged with decreasing film thickness while the spin magnetic moment decreases. Mechanism for the formation of the orbital magnetic moment is discussed based on the electronic structure of the compressively strained SRO film.

PACS numbers: 71.30.+h, 75.70.Ak, 75.30.Kz, 78.70.Dm

I. INTRODUCTION

SrRuO₃ (SRO), a 4d transition metal oxide with the perovskite-type structure, is a ferromagnetic metal with a relatively high Curie temperature of $T_c \sim 160$ K. The electrical resistivity does not saturate even above 500 K, where the Ioffe-Regel limit is exceeded^{1,2}, indicating highly incoherent nature of the metallic state, i.e., so-called a “bad metallic” behavior. From the device application point of view, SRO is a promising material, e.g., as electrodes because of the chemical stability and the structural compatibility with many functional oxides.

It has been known that the electronic and magnetic properties of epitaxially grown thin films are profoundly affected by the film thickness and the epitaxial strain from the substrates. Several studies have shown that, with decreasing film thickness, SRO thin films exhibit a metal-to-insulator transition and concomitant loss of ferromagnetism at a critical thickness of several monolayer (ML)³⁻⁵. Using the laser molecular beam epitaxy (MBE) method, Toyota *et al.*^{3,4} reported the thickness-dependent electronic structure of SRO films grown on Nb-doped SrTiO₃(001) (Nb:STO) substrates by measuring the electrical resistivity and valence-band photoemission spectra. They showed from the temperature dependence of the resistivity that the films changed from metallic to insulating with decreasing thickness. The photoemission spectra of the SRO thin films showed a clear Fermi edge for film thicknesses above 5 ML. With decreasing film thickness, the center of the Ru 4d band moved towards higher binding energies and the intensity at the Fermi level (E_F) decreased, resulting in an energy

gap opening at the E_F below 4 ML. This indicates that SRO thin film undergoes a metal-insulator transition between 4 ML and 5 ML thicknesses, consistent with the resistivity measurements. The magnetic properties of SRO thin films grown on STO(001) substrates have been investigated by Xia *et al.* through magneto-optical Kerr effect measurements⁵. With decreasing film thickness, the film showed a transition from ferromagnetic to paramagnetic between 4 ML and 3 ML. Mahadevan *et al.*⁶ performed a density-functional calculation, and found that the SRO film indeed exhibits a thickness-dependent transition from a ferromagnetic metal to an antiferromagnetic insulator at 4 ML. As for the magnetic anisotropy, the magnetic moment was found nearly perpendicular to the film surface. With increasing in-plane lattice constant through increasing the Ba content in (Ba,Sr)TiO₃ (BSTO) substrates, the easy magnetization axis changed from out-of-plane to in-plane⁷.

It has been generally considered that perpendicular magnetic anisotropy arises from magneto-crystalline anisotropy caused by spin-orbit interaction. Bruno has shown that the MCA energy is proportional to the difference in the orbital magnetic moment between the perpendicular and in-plane directions⁸, and this has been confirmed for 3d transition metals such as Au/Co/Au(111) thin films⁹ and FeCo/Ni multilayers¹⁰. If the Bruno theory is applicable to Ru compounds, too, the SRO thin films grown on STO are expected to exhibit a finite orbital magnetic moment perpendicular to the plane although the orbital magnetic moment in bulk SRO has been reported to be negligibly small¹¹. So far, different values have been reported for the orbital magnetic mo-

ment of Ru in SRO thin films grown on STO substrates not only with (001) surfaces but also with (110) and (111) surfaces^{12,13} and the issue still remains controversial.

The purpose of the present study is to elucidate the thickness-dependent magnetic properties of the SRO thin films grown on STO(001) substrates through the measurements of the spin and orbital magnetic moments using X-ray magnetic circular dichroism (XMCD). We indeed observed a finite orbital magnetic moment of $\sim 0.1 \mu_B/\text{Ru}$ atom perpendicular to the film surface. The origin of the perpendicular orbital magnetic moment, which should be related to the perpendicular magnetic anisotropy according to Bruno⁸, shall be discussed.

II. EXPERIMENT

SRO thin films were fabricated on TiO_2 -terminated 0.05% Nb-doped STO(001) substrates by the laser-MBE method with precise control of thickness. The wet-etched STO(001) substrates with TiO_2 -termination were annealed at 1100 °C for 2 hours under an oxygen pressure of 1×10^{-7} Torr to ensure atomically flat surfaces. Sintered SRO pellets were used as targets. A Nd:YAG (yttrium aluminum garnet) laser was used for ablation in its frequency-tripled mode ($\lambda = 355$ nm) at a repetition rate of 1 Hz. During the deposition, the substrate temperature was kept at 750 °C and the oxygen pressure at 1×10^{-3} Torr. The thickness of thin films were determined by reflection high-energy electron-diffraction (RHEED) oscillation. The RHEED pattern showed Kikuchi lines and no three-dimensional Bragg spots, which means that the SRO thin films have flatter surfaces and are better crystallized than those fabricated in previous works^{3,4}. *Ex situ* atomic force microscope studies showed step-and-terrace structures for all the samples. For the samples with 4-8 ML thickness, however, the step edges were irregular, which means that the step-flow growth condition was not achieved¹⁴. The pseudo-cubic lattice constant of SRO is ~ 3.92 Å and is larger than the lattice constant 3.905 Å of STO by 0.4%, meaning that the SRO thin films grown on STO substrates are under compressive strain.

Soft x-ray photoemission measurements were performed at the undulator beamline BL-2C of Photon Factory, KEK. X-ray absorption spectroscopy (XAS) and XMCD measurements were performed at the helical undulator beamline BL23SU of SPring-8 except for the sample of 50 ML thickness. As for the sample of 50 ML thickness, XAS and XMCD measurements were performed at the undulator beamline BL-16A of Photon Factory, KEK. For the samples measured at SPring-8, in order to eliminate spurious signals in XMCD spectra, the helicity of the incident circularly polarized light was switched at each photon energy, and two XMCD spectra obtained using opposite magnetic-field directions were averaged. The Ru $M_{2,3}$ -edge (Ru $3p \rightarrow 4d$) XAS and XMCD spectra were taken at 20 K by the total electron yield mode with

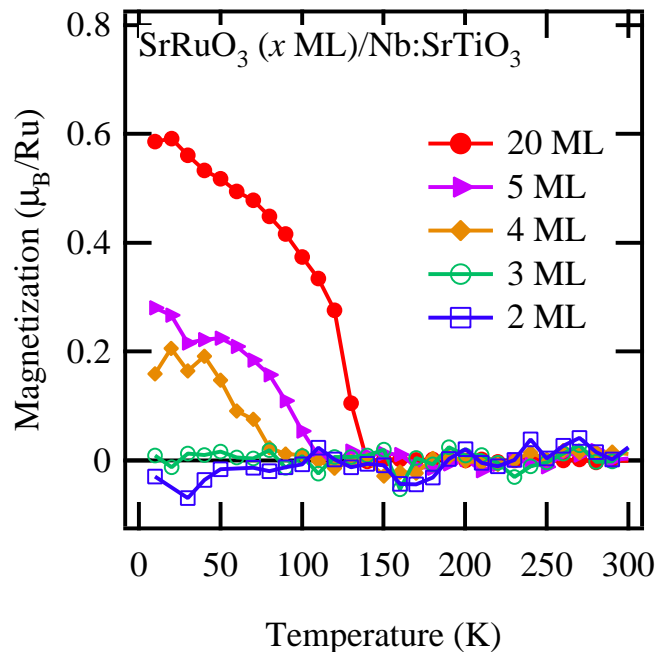


FIG. 1. (Color online) Temperature dependence of the magnetization of SrRuO_3 thin films grown on Nb:STO substrates with various thicknesses measured by remnant magnetization after field cooling at $\mu_0 H = 3$ T. The films with thicknesses greater than 4 ML show ferromagnetic behavior.

negative bias. External static magnetic field of 0.1-5 T was applied perpendicular to the film surfaces.

III. RESULT AND DISCUSSION

Magnetization-temperature curves of the SRO films with various thicknesses were measured using a superconducting quantum interference device (SQUID) and are shown in Fig. 1. They show that the magnetization quickly increases above 4 ML, indicating that a paramagnetic-ferromagnetic transition occurs between 3 and 4 ML thicknesses.

Photoemission spectra in the valence-band region are shown in Fig. 2(a). One can see three structures originating from the O $2p$ band, one of which is located around 4 eV and the others are located around 7 eV and 8 eV^{15,16}. Photoemission within ~ 2 eV of E_F is originated from the Ru $4d$ band¹⁶. The spectrum for the film thicknesses of 2 ML exhibits an energy gap at E_F , as clearly seen in the spectra near E_F [Fig. 2(b)]. The leading edge of the Ru $4d$ band reaches E_F at 3 ML and the Fermi edge is established at 4 ML, indicating a thickness-dependent insulator-to-metal transition at a critical film thickness between 3 and 4 ML. This critical thickness is the same as that reported in Ref. 5 but by 1 ML smaller than that reported in Refs. 3 and 4.

Figure 3 shows the Ru $M_{2,3}$ XAS and XMCD spec-

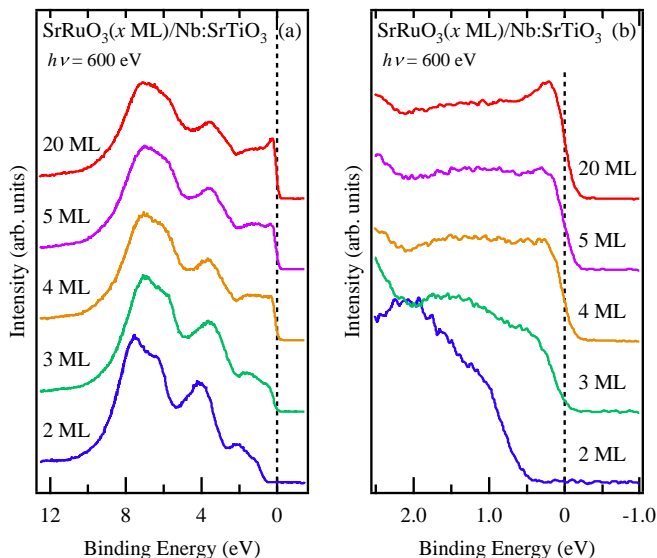


FIG. 2. (Color online) Thickness dependence of the *in situ* valence-band photoemission spectra of SrRuO₃ thin films grown on Nb-doped SrTiO₃ substrates. (a) The entire valence band, and (b) near E_F region. The Fermi cutoff is clearly seen above 3 ML¹⁴, indicating the metallic nature of the films.

tra of the 50 ML and 4 ML SRO films at the magnetic field of $\mu_0 H = 5.0$ T. For the 50 ML-thick SRO film [Fig. 3(a)], clear Ru M_{2,3} XAS and XMCD spectra were observed. For the 4 ML-thick film [Fig. 3(b)], the strong Ti L_{2,3}-derived peaks from the STO substrate overlap the Ru M₃ ($3p_{3/2} \rightarrow 4d$) peak because the SRO thickness of 4 ML was not thick enough compared with the probing depth of XAS. On the other hand, the Ru M₂ ($3p_{1/2} \rightarrow 4d$) edge at 484.4 eV does not overlap the Ti L_{2,3} edge, and is therefore better resolved. The Ru M₃ edge XAS buried under the Ti L_{2,3} XAS is deduced from the Ru M₂ peak intensity, and is plotted, by a dashed curve in Fig. 3(b). Taking the difference between the XAS spectra for right and left circularly polarized light, we have obtained the XMCD spectra as shown in the bottom panels of Figs. 3(a) and (b). In Fig. 3(b), despite the strong XAS signals from the Ti L_{2,3} edge, no spurious XMCD signals due to the Ti L_{2,3} XAS are detected. Since the XMCD spectrum in Fig. 3(b) was measured by reversing the photon helicity at each photon energy and also by reversing the magnetic field, we consider that the intrinsic Ru M_{2,3} XMCD of SRO was clearly observed.

Figure 4 shows thus obtained Ru M₂-edge XMCD spectra of SRO films with various thicknesses taken at the low magnetic field of $\mu_0 H = 0.1$ T. In such a low magnetic field, while ferromagnetic samples show strong XMCD signals paramagnetic samples show only very weak XMCD signals. One can see that the XMCD intensity decreases with decreasing film thickness and vanishes at 3 ML, signaling a ferromagnetic-to-paramagnetic transition between 4 ML and 3 ML. The thickness and magnetic-field dependences of the Ru M₂-edge XMCD

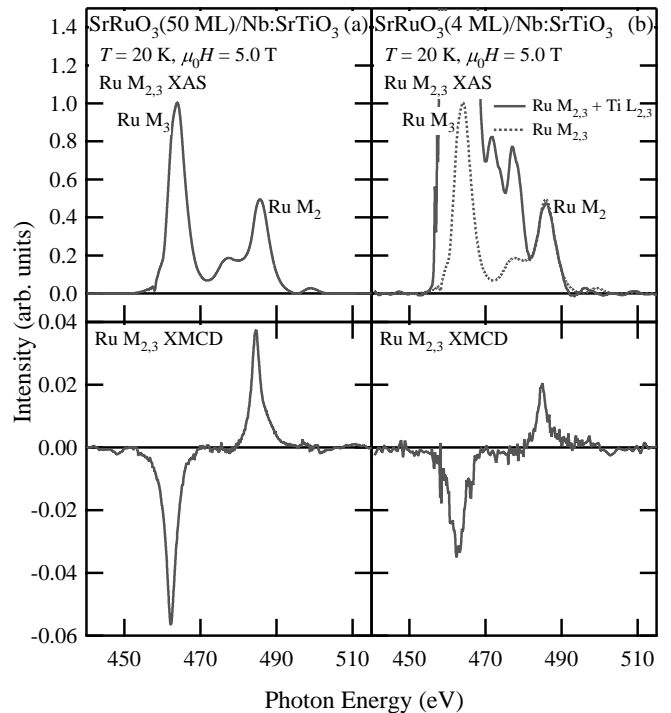


FIG. 3. (Color online) Ru M_{2,3}-edge XAS and XMCD spectra of SrRuO₃ thin films with the thicknesses of 50 ML (a) and 4 ML (b). The dashed curves in panel (b) is the XAS spectrum of the 50 ML film plotted so that the Ru M₂ intensities coincide.

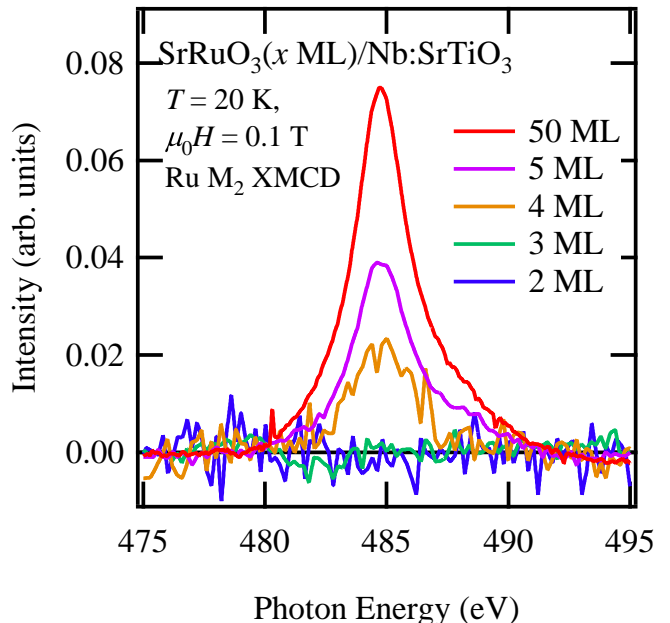


FIG. 4. (Color online) Thickness dependence of the Ru M₂-edge XMCD spectra of SrRuO₃ thin films. The intensities have been normalized to the Ru M₂-edge XAS intensity.

intensity were measured and are summarized in Fig. 5. According to Fig. 5(a), the XMCD intensity of the 3 ML film show an increase at high magnetic fields, indicating a paramagnetic (or an antiferromagnetic) ground state and a possible metamagnetic behavior. The XMCD intensities of the 4 ML and thicker films, on the other hand, show an abrupt increase from $\mu_0 H = 0$ T to almost saturated values at $\mu_0 H = 0.1$ T, confirming that these films are ferromagnetic. Figure 5(b) is the thickness dependence of XMCD intensities at several fixed magnetic fields. They all show increase with film thickness above 4 ML at all applied fields.

The thickness and magnetic-field dependences of the orbital and spin magnetic moments have been derived using the XMCD sum rules^{17,18} and are plotted in Fig. 6. The spin magnetic moment of the thick SRO films is comparable to that of bulk SRO sample¹¹ ($m_{\text{spin}} \simeq 0.6 \mu_B/\text{Ru}$). This does not follow the result of first-principles calculation on SRO under epitaxial strain which indicates that the magnetic moment should decrease by $\sim 10\%$ under the compressive strain of 0.4% from the STO substrate¹⁹, probably because the accuracy of the previous XMCD measurements on bulk SRO crystal¹¹ was not sufficient to discuss the subtle differences between the bulk and thin film data.

The orbital magnetic moment ($m_{\text{orb}} \simeq 0.08 \mu_B/\text{Ru}$) of the thick SRO film is much smaller than 0.2-0.3 μ_B reported in the previous Ru $M_{2,3}$ XMCD study of SRO films grown on STO(001) and (111) substrates¹² but significantly larger than that ($m_{\text{orb}} \simeq 0.0-0.03 \mu_B/\text{Ru}$) reported by the very recent XMCD study at the Ru $L_{2,3}$ edge XMCD of SRO films grown on STO(001) and (111)¹³. The discrepancy between the Ru $L_{2,3}$ edge and the present $M_{2,3}$ edge studies even without overlapping Ti $L_{2,3}$ edges may be due to the large (~ 130 eV) spin-orbit splitting of the Ru $L_{2,3}$ edge which may make the transition-matrix elements for the L_2 and L_3 edges slightly different. Because the XMCD sum rules have been derived under the assumption that the radial part of the core-level wave functions is the same for the $j = l + 1/2$ and $l - 1/2$ core levels, it may be different if the spin-orbit interaction is very strong. If the L_2 edge has a larger (smaller) matrix element than L_3 , the orbital magnetic moment will be underestimated (overestimated). The reason why the m_{orb} value reported in Ref. 12 is much larger than ours is not known at present. This discrepancy may be related to the unusually large m_{spin} value ($\sim 3.4 \mu_B/\text{Ru}$) reported in Ref. 12 compared to ours ($\sim 0.6 \mu_B/\text{Ru}$) as well as to the value deduced from bulk magnetization measurements ($\sim 1.0 \mu_B/\text{Ru}$)¹¹. As for the 4 ML film, since the spin magnetic moment is smaller ($m_{\text{spin}} \simeq 0.4 \mu_B/\text{Ru}$) than that of bulk SRO, the ratio $m_{\text{orb}}/(m_{\text{spin}} + 7m_T)$ is larger in the thin film than in the 50 ML thick film by a factor of ~ 2 , as plotted in Fig. 6.

The finite orbital magnetic moment perpendicular to the film can be understood from the band structure of SRO as follows: In SRO, the t_{2g} band is partially oc-

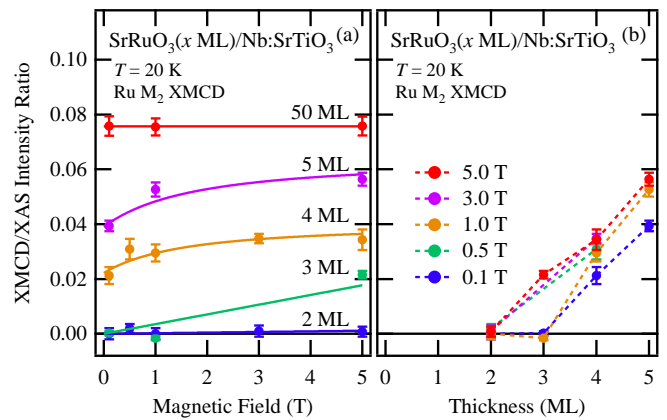


FIG. 5. (Color online) Thickness (a) and magnetic-field (b) dependences of the XMCD intensities (measured in terms of the XMCD/XAS intensity ratio) at the Ru M_2 edge of SrRuO₃ thin films.

cupied and spin-polarized while the e_g band is empty. Under the compressive strain, the t_{2g} band is split into the wider d_{xy} band and the narrower doubly degenerate d_{yz}/d_{zx} bands. When the spins are perpendicular to the film, i.e., along the z direction, the d_{yz} and d_{zx} bands are mixed through (the $L_z S_z$ term of) the spin-orbit interaction, and the orbital magnetic moment along the z direction is induced. When the spins are parallel to the film, e.g., along the x direction, the d_{zx} and d_{xy} bands are mixed through (the $L_x S_x$ term of) the spin-orbit interaction, and the orbital magnetic moment is induced along the x direction, however, the induced orbital moment is smaller because the wider d_{xy} band is involved.²⁰ According to Bruno⁸, the larger orbital magnetic moment perpendicular to the film than that parallel to it should lead to the perpendicular magnetic anisotropy, as confirmed by XMCD for several systems including Co thin films sandwiched by Au(111).⁹ For the Au/Co/Au(111) film, the orbital magnetic moment perpendicular to the film increases with decreasing Co film thickness.⁹ In the case of the SRO thin films, the increase of the ratio $m_{\text{orb}}/(m_{\text{spin}} + 7m_T)$ with decreasing film thickness may be induced by a similar mechanism to the Au/Co/Au film. In order to see whether Bruno's theory⁸ holds or not for the SRO films, the orbital magnetic moment parallel to the film as well as the orbital magnetic moment of SRO thin films grown on substrates having different lattice constants such as BSTO⁷ remain to be measured in the future. On the theoretical side, first-principles calculation on SRO thin films explicitly including the Ru $4d$ spin-orbit coupling (~ 150 meV), which is larger than that of Co $3d$ (~ 70 meV), is necessary to quantitatively understand the origin of the perpendicular orbital magnetic moment and the perpendicular magnetic anisotropy.

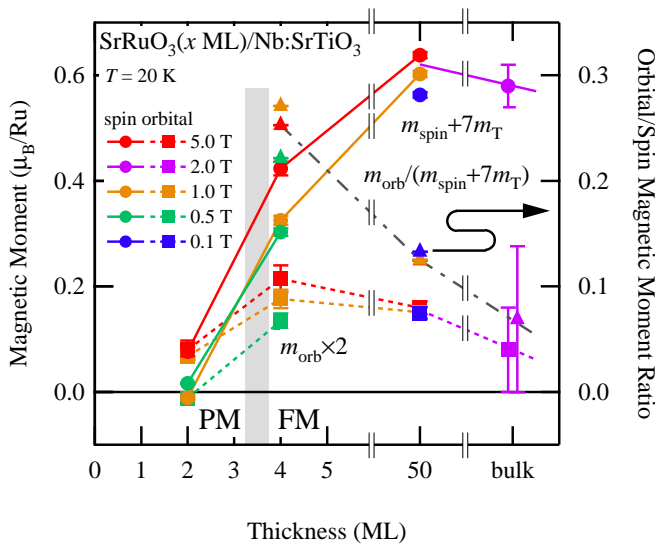


FIG. 6. (Color online) Magnetic-field dependence of the (effective) spin magnetic moments ($m_{\text{spin}} + 7m_{\text{T}}$) and the orbital magnetic moments (m_{orb}) of SrRuO_3 thin films. The electron occupation number n_{4d} is assumed to be 4. m_{T} is the expected value of the magnetic dipole operator which originate from the anisotropic distribution of the spin density. The data of bulk SrRuO_3 are taken from Ref. 11.

IV. SUMMARY

We have performed XMCD measurements on the SRO thin films with various thicknesses grown on STO(001) substrates. With decreasing film thickness, the intensity of the XMCD spectra decreased and the XMCD signal at low magnetic field became very weak below 3 ML, indicating a ferromagnetic-to-paramagnetic transition. While films with thicknesses larger than 4 ML showed strong, magnetic-field-independent XMCD, indicating ferromagnetic behavior, the sample with 3 ML thicknesses showed weak XMCD signals which increases with magnetic field, consistent with (enhanced) paramagnetic behavior. The orbital magnetic moment perpendicular to the film was found to be small but finite ($\sim 0.1 \mu_{\text{B}}/\text{Ru}$). The origin of the perpendicular orbital magnetic moment is discussed based on the band structure of SRO under the compressive strain.

ACKNOWLEDGMENTS

We would like to thank Kenta Amemiya and Masako Sakamaki for valuable technical support at KEK-PF. Discussion with P. Mahadevan is gratefully acknowledged. This work was supported by a Grant-in-Aid for Scientific Research from JSPS (S22224005) and the Quantum Beam Technology Development Program from JST. The experiment was performed under the approval of the Photon Factory Program Advisory Committee (Proposal Nos. 2009G579, 2012G667, 2013S004) and under the Shared Use Program of JAEA Facilities (Proposal Nos. 2011A3840/BL23SU).

- ¹ P. Li, F. E-Hua, X. Ying, and Z. Yu-Heng, Chinese Phys. Lett. **23**, 2225 (2006).
- ² L. Pi, A. Maignan, R. Retoux, and B. Raveau, J. Phys.: Condens. Matter **14**, 7391 (2002).
- ³ D. Toyota, I. Ohkubo, H. Kumigashira, M. Oshima, T. Ohnishi, M. Lippmaa, M. Takizawa, A. Fujimori, K. Ono, M. Kawasaki, and H. Koinuma, Appl. Phys. Lett. **87**, 162508 (2005).
- ⁴ D. Toyota, I. Ohkubo, H. Kumigashira, M. Oshima, T. Ohnishi, M. Lippmaa, M. Kawasaki, and H. Koinuma, J. Appl. Phys. **99**, 08N505 (2006).
- ⁵ J. Xia, W. Siemons, G. Koster, M. R. Beasley, and A. Kapitulnik, Phys. Rev. B **79**, 140407 (2009).
- ⁶ P. Mahadevan, F. Aryasetiawan, A. Janotti, and T. Sasaki, Phys. Rev. B **80**, 035106 (2009).
- ⁷ K. Terai, T. Ohnishi, and M. L. K. Kawasaki, Jpn. J. Appl. Phys. **43**, 227 (2004).
- ⁸ P. Bruno, Phys. Rev. B **39**, 865 (1989).
- ⁹ D. Weller, J. Stöhr, R. Nakajima, A. Carl, M. G. Samant, C. Chappert, R. Mégy, P. Beauvillain, P. Veillet, and G. A. Held, Phys. Rev. Lett. **75**, 3752 (1995).
- ¹⁰ J. M. Shaw, H. T. Nembach, and T. J. Silva, Phys. Rev. B **87**, 054416 (2013).
- ¹¹ J. Okamoto, T. Okane, Y. Saitoh, K. Terai, S.-I. Fujimori, Y. Muramatsu, K. Yoshii, K. Mamiya, T. Koide, A. Fujimori, Z. Fang, Y. Takeda, and M. Takano, Phys. Rev. B **76**, 184441 (2007).
- ¹² A. J. Grutter, F. J. Wong, E. Arenholz, A. Vailionis, and Y. Suzuki, Phys. Rev. B **85**, 134429 (2012).
- ¹³ S. Agrestini, Z. Hu, C.-Y. Kuo, M. W. Haverkort, K.-T. Ko, N. Hollmann, Q. Liu, E. Pellegrin, M. Valvidares, J. Herrero-Martin, P. Gargiani, P. Gegenwart, M. Schneider, S. Esser, A. Tanaka, A. C. Komarek, and L. H. Tjeng, Phys. Rev. B **91**, 075127 (2015).
- ¹⁴ D. Toyota, Master Thesis, (The University of Tokyo, 2006).
- ¹⁵ J. Okamoto, T. Mizokawa, A. Fujimori, I. Hase, M. Nohara, H. Takagi, Y. Takeda, and M. Takano, Phys. Rev. B **60**, 2281 (1999).
- ¹⁶ D. Kobayashi, H. Kumigashira, M. Oshima, T. Ohnishi, M. Lippmaa, K. Ono, M. Kawasaki, and H. Koinuma, J. Appl. Phys. **96**, 7183 (2004).
- ¹⁷ B. T. Thole, P. Carra, F. Sette, and G. van der Laan, Phys. Rev. Lett. **68**, 1943 (1992).
- ¹⁸ P. Carra, B. T. Thole, M. Altarelli, and X. Wang, Phys. Rev. Lett. **70**, 694 (1993).

¹⁹ A. T. Zayak, X. Huang, J. B. Neaton, and K. M. Rabe, Phys. Rev. B **77**, 214410 (2008).

²⁰ If the SRO film is grown under tensile strain (as in the case of Ref. 7), the t_{2g} band is split into the narrower d_{xy} band and the wider d_{yz}/d_{zx} bands, and the magnitude of the

orbital magnetic moment would be larger for the in-plane spin direction, for which the narrower d_{xy} band is involved in the spin-orbit coupling.